

TRANSPORT OF A CONDENSABLE SPECIES IN NONISOTHERMAL TUBE FLOW

YOUNG KAG KIM† AND SANG SOO KIM‡

†*Production Engineer Center, Samsung Display Devices Co., Ltd., 575 Shin-ri, Taean-eub, Hwasung-kun, Kyungki-do, 445-970, Korea*

‡*Department of Mechanical Engineering, Korea Advanced Institute of Science and Technology, 373-1 Kusong-dong, Yusong-gu, Taejon, 305-701, Korea*

ABSTRACT

We present the equations for condensation in cooled upward laminar flow in tubes and consider their solution for low vapour concentrations and variable vapour-gas thermodynamic properties. We treated the full problem, including coupling with the aerosol size distribution, by using the PSI-CELL (Particle Source in Cell) method. The particle trajectories start from the point where the particles are generated by homogeneous nucleation. Particle size distribution and vapour scavenging by particles are obtained in forced convection and mixed convection regions. Calculations were also conducted with respect to tube diameters.

KEY WORDS Vapour Particle Mixed convection flow Homogeneous nucleation Seed particle

NOMENCLATURE

A	sectional area of tube [m ²]	r'	nondimensional radial distance (r/D)
C_c	Cunningham correction factor ($1 + Kn(1.257 + 0.4 \exp(-1.1/Kn))$)	Re	Reynolds number ($u_{in}D/v_{in}$)
d	diameter of a particle [m]	S	supersaturation ratio (p_e/p_s)
d_i	molecular diameter of condensable species [m]	t	time [s]
d'	nondimensional diameter of a particle (d/d_i)	T	temperature [°K]
D	diameter of tube [m]	T'	nondimensional temperature (T/T_{in})
D_v	vapour diffusivity [m ² /s]	u	gas velocity [m/s]
g	gravitation acceleration [m/s ²]	u'	nondimensional gas velocity (u/u_{in})
G	condensational growth rate [m ³ /s]	v	volume of a particle [m ³]
I	nucleation rate [1/m ³ s]	v_m	molecular volume of condensable species [m ³]
K	thermophoretic coefficient	V_{cell}	grid cell volume [m ³]
Kn	Knudsen number based on gas ($2\lambda/d$)	z	axial coordinate [m]
Kn_v	Knudsen number based on condensable species ($2\lambda_v/d$)	z'	nondimensional axial coordinate ($(z/D)/RePr$)
m	molecular mass of condensable species [kg]	α	thermal diffusivity [m ² /s]
n_i	particle number density for class i [1/m ³]	σ	surface tension [N/m]
\dot{n}_i	particle number flux for class i [1/s]	δ	delta function
p_v	vapour pressure [N/m ²]	κ	Boltzmann's constant (1.380662×10^{-23} J/°K)
p_s	saturation vapour pressure [N/m ²]	λ	mean free path of gas [m]
P	total pressure [N/m ²]	λ_v	mean free path of condensable species [m]
Pr	Prandtl number for heat transfer (v_{in}/α_{in})	μ	viscosity [kg/m s]
r	radial distance [m]	ν	kinematic viscosity [m ² /s]
		θ^*	nondimensional temperature ($(T_w)/(T_{in} - T_w)$)
		ρ	gas density [kg/m ³]

0961-5539/95/090797-16\$2.00
© 1995 Pineridge Press Ltd

Received September 1993
Revised February 1995

τ	viscous stress [N/m^2]	<i>Subscripts</i>
ω_v	vapour mass fraction (ρ_v/ρ)	<i>in</i>
ω'_v	nondimensional vapour mass fraction ($\omega_v - \omega_{v,n}$)/($\omega_{v,m} - \omega_{v,n}$)	<i>p</i>
ω_p	particle mass fraction ($\sum \rho_p v_i n_i/\rho$)	<i>r</i>
ω'_p	nondimensional particle mass fraction (ω_p)/($\omega_{v,m} - \omega_{v,n}$)	<i>v</i>
		<i>w</i>
		<i>z</i>
		seed
		seed particles

INTRODUCTION

Aerosol processes are relevant to a variety of fields such as the fabrication of optical wave guides and semiconductor devices, the design of gas cleaning devices, particle measuring equipment and aerosol generators. Aerosol dynamics are described by the so-called general dynamic equation¹. Such processes include coagulation, growth due to condensation of vapours, shrinkage due to evaporation, nucleation of new aerosols, sedimentation, and deposition on surfaces. Many approaches have been developed to simulate aerosol dynamics^{2,3}.

The process of condensation growth is analogous to an advection process, and presents a notoriously difficult problem to solve numerically, by the Eulerian method, because of a tendency for numerical diffusion and dispersion to arise and accurate numerical modelling by the Eulerian method is a formidable job^{4,5}. If a specific function for particle size distribution or monodispersity is assumed, the Eulerian method in particle size distribution (PSD) equation is available⁶. However, the real PSD cannot be represented by a specific mathematical function⁷. If the particle size distribution function is not assumed, the numerical diffusion and dispersion in the Eulerian method are severe. Thus, for aerosol dynamics considering only condensation, a numerical method on the Lagrangian employing approach is the preferred option⁴.

For conditions of monodispersity, the flow condition in the condenser of a continuous flow condensation particle generator is mainly that of mixed convection⁸. Vapour scavenging by particles in a mixed convection region is very different from that in the forced convection flow because particle trajectories are not parallel to the tube axis and their paths depend on their sizes and local positions. In this study, the flow region is extended from a forced convection dominated region to a mixed convection region. We consider the steady state laminar flow of an aerosol-vapour-gas mixture along the vertical cooled tube with an upward flow direction. The heat and momentum transfer equations are not coupled with the equation of the aerosol size distribution. We include homogeneous nucleation, condensation to particles in addition to wall condensation for Na_2SO_4 vapour-air mixtures with and without seed particles. The coupling effects of particle and vapour conservation equations are obtained by PSI-CELL (particle source in cell) method⁹.

GOVERNING EQUATIONS

We consider the convective flow of a stream, containing a trace amount of condensable vapour, through a vertical cooled tube with an upward flow direction. The inlet stream is saturated with respect to the vapour, the concentration of which is sufficiently dilute ($\omega_v < 10^{-3}$) to render negligible the effects of condensation on heat transfer and fluid mechanics. The latent heat effect due to vapour condensation in an energy equation is assumed to be negligible because the amount of condensable vapour is very minute. The particle phase momentum and thermal relaxation times are several orders of magnitude smaller than the relevant characteristic flow time, and, moreover, the volume fraction of particles is very low. This means that, in the absence of external forces, the particle velocity and temperature will be identical to the local gas velocity and temperature. Because of these facts we can ignore the presence of particles when calculating

the velocity and temperature profiles. Here, radiation heat flux and the chemical interactions between vapour and seed particles are neglected.

The governing equations in the cylindrical coordinate system can be written as,

Continuity:

$$\frac{1}{r} \frac{\partial}{\partial r} (r\rho u_r) + \frac{\partial}{\partial z} (\rho u_z) = 0, \tag{1}$$

Momentum:

$$\frac{1}{r} \frac{\partial}{\partial r} (r\rho u_r u_r) + \frac{\partial}{\partial z} (\rho u_z u_r) = -\frac{\partial P}{\partial r} - \frac{1}{r} \frac{\partial}{\partial r} (r\tau_{rr}) - \frac{\partial \tau_{rz}}{\partial z}, \tag{2}$$

$$\frac{1}{r} \frac{\partial}{\partial r} (r\rho u_r u_z) + \frac{\partial}{\partial z} (\rho u_z u_z) = -\frac{\partial P}{\partial z} - \frac{1}{r} \frac{\partial}{\partial r} (r\tau_{rz}) - \frac{\partial \tau_{zz}}{\partial z} - \rho g, \tag{3}$$

Energy:

$$\frac{1}{r} \frac{\partial}{\partial r} (r\rho u_r T) + \frac{\partial}{\partial z} (\rho u_z T) = \frac{1}{Pr} \left(\frac{1}{r} \frac{\partial}{\partial r} \left(r\mu \frac{\partial T}{\partial r} \right) + \frac{\partial}{\partial z} \left(\mu \frac{\partial T}{\partial z} \right) \right). \tag{4}$$

The effects of buoyancy and variable properties, being functions of the temperature, are included with the density and viscosity. The density ρ is obtained from the ideal gas law and the total pressure is atmospheric. The Prandtl number is constant and the viscosity is obtained from the Sutherland's approximation¹⁰.

The boundary conditions are,

$$\begin{aligned} u_r = 0, \quad \frac{\partial u_z}{\partial r} = \frac{\partial T}{\partial r} = 0 & \quad \text{at } r = 0, \\ u_z = u_r = 0, \quad T = T_w & \quad \text{at } r = D/2, \\ u_z = 2u_{in}(1 - (2r/D)^2), \quad u_r = 0, \quad T = T_{in} & \quad \text{at } z = 0, \\ \frac{\partial^2 u_z}{\partial z^2} = \frac{\partial^2 u_r}{\partial z^2} = \frac{\partial^2 T}{\partial z^2} = 0 & \quad \text{at exit.} \end{aligned} \tag{5}$$

Here, we assume that the inlet velocity is fully developed and the inlet temperature is uniform. At the outlet plane the second derivatives in the axial direction of the dependent variables are set equal to zero.

Particle flux

In a subcooled region, the supersaturation ratio may exceed the critical value for the onset of homogeneous nucleation in a dust-free gas. This results in the formation of finite-sized particles. The classical Becker-Doering nucleation theory is employed to calculate the homogeneous nucleation rate (I):

$$I = 2 \left(\left(\frac{\sigma}{2\pi m} \right) \left(\frac{p_v}{\kappa T} \right)^2 v_m \right) \exp \left(-\frac{\pi \sigma d^{*2}}{3\kappa T} \right) \delta(d - d^*), \tag{6}$$

$$d^* = \frac{4\sigma v_m}{\kappa T \ln(S)}. \tag{7}$$

In this case, the particle flux can be represented by,

$$\dot{n}_i = I \cdot V_{cell}. \tag{8}$$

For seed particles, we assume that the inlet velocities of seed particles are equal to the inlet gas velocity. The particle flux can be represented by,

$$\dot{n}_i = \int_{A_i} n_{i,m} u_{z,m} dA, \quad (9)$$

where A_i is the area of the inlet port. The number concentrations of particles are sufficiently low so that coagulation can be neglected¹¹, and thus \dot{n}_i is conserved along their path.

Particle growth

For particle growth rate by direct vapour condensation, we adopt a well-known approximate interpolation formula for the entire range of mean free path¹:

$$G = \frac{dv}{dt} = \frac{2\pi D_v dv_m}{\kappa T} \left(p_v - p_s \exp\left(\frac{4\sigma v_m}{d\kappa T}\right) \right) F. \quad (10)$$

The second term on the right hand side represents Kelvin's effect and the Fuchs and Sutugin correction factor, F , is represented by¹²,

$$F = \frac{1 + Kn_v}{1 + 1.71Kn_v + 1.333Kn_v^2}, \quad (11)$$

where Kn_v is the Knudsen number of the condensing species. We ignore the effects of surface properties on the initial condensation (heterogeneous nucleation) process and assume that (10) applies right down to the condensation nucleus radius.

Thermophoretic velocity

A particle suspended in a gas with an imposed temperature gradient experiences a thermal force producing motion directed toward the lower temperature. The thermophoretic velocity may be written in the following form¹³:

$$u_T = -\frac{Kv}{T} \nabla T, \quad (12)$$

where K is the thermophoretic coefficient and is assumed to be 0.53.

Vapour conservation equation

The vapour conservation equation is strongly linked to the PSD through the source term for homogeneous nucleation and condensations. The vapour conservation equation can be written as,

$$\frac{1}{r} \frac{\partial}{\partial r} (r\rho(u_r + u_{T,r})\omega_v) + \frac{\partial}{\partial z} (\rho(u_z + u_{T,z})\omega_v) = \frac{1}{r} \frac{\partial}{\partial r} \left(r\rho D_v \frac{\partial \omega_v}{\partial r} \right) + \frac{\partial}{\partial z} \left(\rho D_v \frac{\partial \omega_v}{\partial z} \right) + S_v, \quad (13)$$

where

$$S_v = - \sum_{i,cell} \frac{\pi}{6} \rho_p (d_{i,out}^3 - d_{i,in}^3) \dot{n}_i / V_{cell}. \quad (14)$$

The vapour source term, S_v , represents the amount of vapour scavenged by particles in the cell⁹. The $u_{T,r}$, $u_{T,z}$ are the radial and axial vapour thermophoretic velocity, respectively. The vapour diffusivity is estimated from the kinetic theory of gases¹⁰, and the properties related to the vapour diffusivity are selected from Reid *et al.*¹⁴. The following boundary conditions, appropriate for a superheated stream and a perfectly absorbing wall, are imposed on ω_v . The boundary conditions

are,

$$\begin{aligned} \frac{\partial \omega_v}{\partial r} = 0 \quad \text{at } r=0, \quad \omega_v = \omega_{v_w} \quad \text{at } r=D/2, \\ \omega_v = \omega_{v_m} \quad \text{at } z=0, \quad \frac{\partial^2 \omega_v}{\partial z^2} = 0 \quad \text{at exit.} \end{aligned} \quad (15)$$

In this boundary conditions, the inlet stream mass fraction is specified at the inlet temperature and the saturated wall mass fraction is specified at the wall temperature.

Particle trajectory equation

The particles grow too rapidly to diffuse radially during their residence time in the condenser. The motion of a particle is determined from the combined effects resulting from thermophoresis, gravity, forced convection and secondary flows. Using a Lagrangian description for the particle motion, the following differential equations are obtained for the particle velocity,

$$\begin{aligned} u_{p,r} = u_r - \frac{K_v \partial T}{T \partial r}, \\ u_{p,z} = u_z - \frac{K_v \partial T}{T \partial z} - \frac{\rho_p d^2 g C_c}{18 \rho v}, \end{aligned} \quad (16)$$

where $u_{p,r}$, $u_{p,z}$ are the radial and axial velocities of a particle, respectively, and the third term in the right hand side of axial velocity equation represents gravitational velocity and C_c is the Cunningham correction factor¹.

NUMERICAL SOLUTION

The numerical procedure employed to solve for the velocity, temperature, vapour fields utilizes the primitive variables, u_r , u_z , ρ , T and ω_v . The resulting discretized transport difference equations of continuity, momentum and energy are solved by the SIMPLE algorithm¹⁵. Calculations were carried out with constant properties and considering the buoyancy effects, and the results were in good agreement with the series solutions of Marner and McMillan¹⁶. With suitable modifications, the computational fluid flow and heat transfer algorithms can be used to obtain solutions for the vapour conservation equation¹⁷. The program for the vapour conservation equation was tested by comparing with the results of Walker *et al.* shown in *Figure 1*¹⁸. A total axial nondimensional length of 0.5 was used to determine the effects of the exit condition. The results were virtually the same as for the 0.7 case.

The vapour concentration, which depends on the mass of the aerosol, couples with the set of equations given by (14). The calculation is begun by solving the vapour field assuming that homogeneous nucleations are not occurring. Using this vapour field, the particle flux from (8)–(9) is calculated and then vapour sources by the particles along their path are obtained in each cell. With these vapour sources, the vapour field is solved again. The new vapour field is used to obtain the new vapour sources. After several iterations, the vapour field equation is satisfied to within a predetermined value and the solution that accounts for the mutual interactions of particles and vapour is obtained. To determine the particle trajectories, (16) was solved by using the second-order Runge-Kutta method after u_r , u_z and T had been obtained from (1)–(5).

In the solution of equation (10), the growth rate of particles is very large even though the temperature and the vapour concentration variations in a cell are small. Therefore, in the calculation of particle growth, using a first-order implicit approach, the vapour concentration and the temperature may be approximated as constant over the time step, equal to their values at the end of the time step. Then (10) is separable. This reduces the task of solving for $v_i(t+dt)$

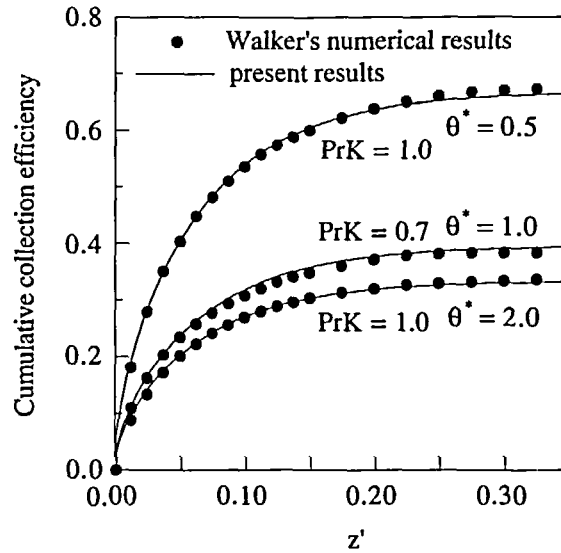


Figure 1 Cumulative collection efficiency along the condenser length

to interpolating on the evolution of a single integral:

$$\int_{v_i(t)}^{v_i(t+\Delta t)} \frac{dv}{G} = \int_t^{t+\Delta t} dt \quad (17)$$

The integral result of (17) allows the removal of some stiffness. In this work, the integral given by (17) is evaluated using Gauss-Legendre quadrature technique¹⁹ and the root of the equation is obtained by using Newton-Raphson method.

For particles generated by homogeneous nucleation, it is assumed that particles are generated with the grid properties in the cell, and a particle flux is described by homogeneous nucleation rate times cell volume. Particles start from the points where the particles are generated. For seed particles, uniform entry of the particles with the flow is approximated by 15 discrete entry locations at every entry grid station. Particle number density in a cell can be described by⁹,

$$n = \sum_i \frac{\dot{n}_i \Delta t_{cell}}{V_{cell}}, \quad (18)$$

where Δt_{cell} is the residence time in the cell and V_{cell} is the cell volume⁹. This method can be easily applied for larger particles for which velocities depend on their size.

Grid sensitivity tests were made for several nonuniform grids, and the values of vapour concentration at several points were found to differ by less than 1 percent between 30×80 and 30×150 grid systems. The 30×80 grid is used in this calculation. Convergence is assumed to be achieved when the maximum residue source of all the equations is less than a threshold (in this study, assigned to 10^{-4} times the fixed flux of the relevant variable at the inlet plane).

RESULTS AND DISCUSSION

All simulations are based on Na_2SO_4 as a condensable vapour. As a carrier gas, air flows through the cooled tube. The range of variables used in this calculation is summarized in Table 1.

Table 1 Parameter range

Medium = air	Condensable species = Na ₂ SO ₄
$\rho_p = 2698 \text{ kg/m}^3$	$T_{in} = 1600^\circ\text{K}$ $T_w = 1400^\circ\text{K}$
$Re = 10\text{--}200$	$\omega_{v,in}$: saturated at T_{in}
$d_{seed} = 0.01 \text{ }\mu\text{m}$	$n_{in} = 10^9\text{--}10^{10}/\text{m}^3$
$\sigma = 6.3995 \times 10^{-1} - 6.648 \times 10^{-4}T + 2.43 \times 10^{-7}T^2 \text{ [N/m]}$	
$\log_{10} p_s = 4.874 - 14,440/T$	$p_s[\text{atm}], T[^\circ\text{K}]$

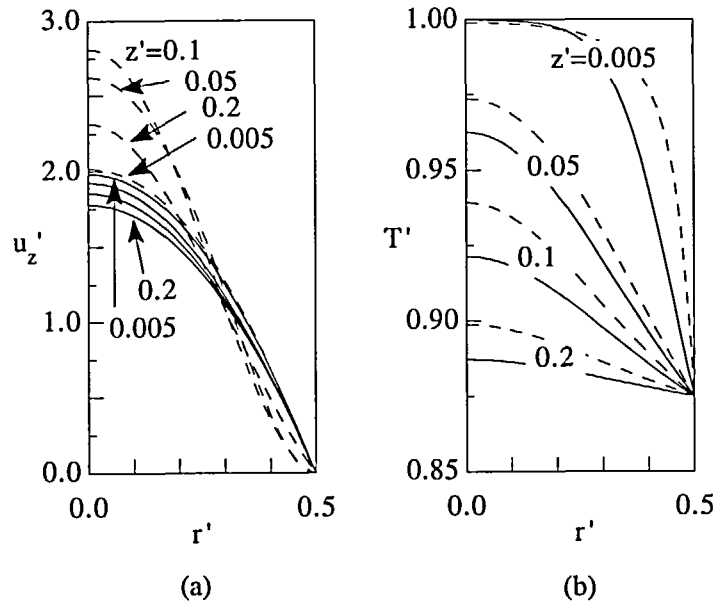


Figure 2 Evolution of radial profiles of axial velocity (a) and temperature (b) along the condenser length for $Re=200$ and $Re=100$ with $D=5 \text{ cm}$ (—, $Re=200$; ---, $Re=100$)

Influence of Reynolds number

Figure 2 shows the nondimensional velocity and temperature profiles for $Re=200$ and 10 in the case of $D=5 \text{ cm}$. The profiles for $Re=200$ and 10 are similar to those in a forced and a mixed convection region, respectively. The temperature profiles for $Re=10$ are more slowly developed than those for $Re=200$.

Vapour concentration and supersaturation ratio for $Re=10$ are more slowly developed than those for $Re=200$ in Figure 3. Vapour concentration around $r'=0.2\text{--}0.3$ is larger than around the wall and the centreline since the vapour diffusion to the wall and vapour condensation to the particles are dominant near the wall and in the centre, respectively. Up to the point of $z'=0.15$ for $Re=200$, the total mass fraction decreases due to the vapour diffusion to the wall. After this point, the total mass fraction along the centreline increases because of the vapour diffusion to the centreline due to the vapour to particle condensation near centreline. Figure 4 presents vapour concentration and supersaturation ratio iso-lines for $D=5 \text{ cm}$ with seed particles, $n_{i,n} = 10^9/\text{m}^3$, and, in this case, homogeneous nucleation is not fully suppressed. The vapour

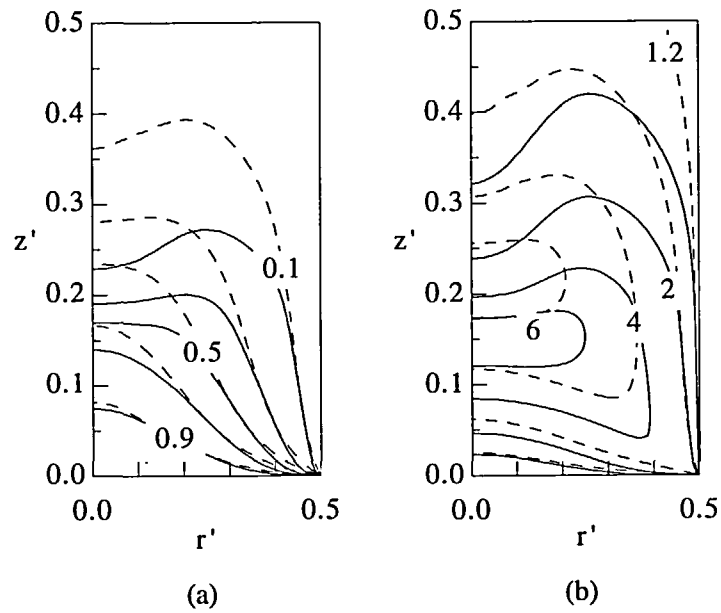


Figure 3 Vapour concentration (ω'_v) (a) supersaturation ratio (S) (b) isopleths with respect to Reynolds number for $D=5$ cm without seed particles (—, $Re=200$; ---, $Re=10$)

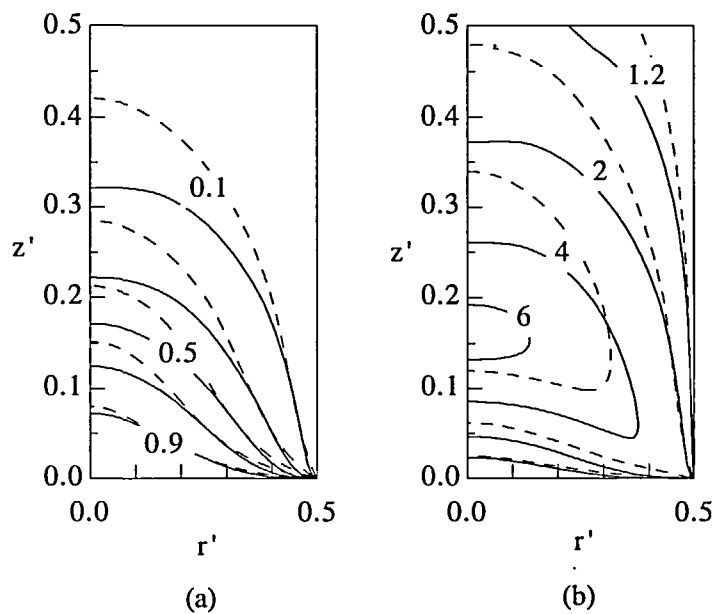


Figure 4 Vapour concentration (ω'_v) (a) and supersaturation ratio (S) (b) isopleths with respect to Reynolds number for $D=5$ cm with seed particles, $n_{i,s}=10^9/m^3$ (—, $Re=200$; ---, $Re=10$)

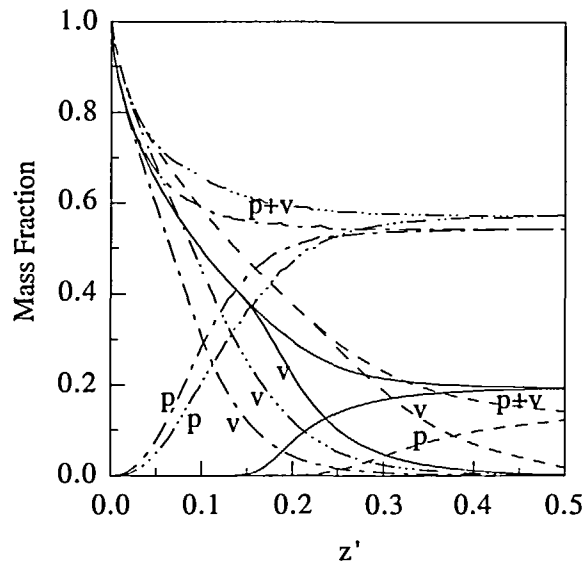


Figure 5 Evolution of particle vapour mass fraction along the condenser length with respect to Reynolds number for $D = 5 \text{ cm}$ (—, $Re = 200$ without seed particles; ---, $Re = 100$ without seed particles; - · - ·, $Re = 200$ with seed particles, $n_{in} = 10^{10}/\text{m}^3$; · · · ·, $Re = 10$ with seed particles, $n_{in} = 10^{10}/\text{m}^3$; p, particle mass fraction (ω_p'); v, vapour mass fraction (ω_v'); p + v, particle + vapour mass fraction ($\omega_p' + \omega_v'$)

concentration profiles are parabolic, which is different from the profiles without seed particles because of the vapour condensation to the seed particles.

In Figure 5, tube average mass fractions are defined by,

$$\bar{\omega}_v = \frac{\int_A \rho u_z \omega_v dA}{\int_A \rho_{in} u_{z,in} \omega_{v,in} dA}, \quad \bar{\omega}_p = \frac{\int_A \rho u_z \omega_p dA}{\int_A \rho_{in} u_{z,in} \omega_{p,in} dA} \tag{19}$$

Without seeding, vapour and total mass concentration for $Re = 10$ are larger than those for $Re = 200$ around the inlet, but total mass fraction for $Re = 10$ becomes smaller than that for $Re = 200$ near the exit. In this system, wall mass loss is mainly governed by the vapour diffusion toward the wall. In the upstream, as Re decreases, the vapour diffusion to the wall decreases and the temperature development is delayed, nucleation and the vapour to particle condensation are also suppressed. Therefore, vapour phase diffusion continues to the exit so that the total mass fraction decreases because the diffusivity of vapour phase is larger than that of particle phase. In order to decrease wall loss, it is shown that a forced convection flow is more favourable than a mixed convection flow. However, with sufficient seed particles in the flow where homogeneous nucleation is fully suppressed, particle mass fraction at the exit is larger in the case of low Re since vapour to particle condensation occurs before the vapour diffuses to the wall.

Recent investigations clearly indicate that, in the condenser tube of an aerosol generator, vapour diffusion to the wall degrades the performance of the aerosol generator²⁰. If vapour wall loss is very large, particle growth rate is reduced and particle size distribution is very disperse. The optimum condition for monodispersity in a condenser tube is the balance of free and forced convection forces which makes the flow profile more shallow⁸. This occurs when all the nuclei have experienced identical growth histories. This can be achieved by reducing the gas flow, but if the flow is reduced too much, the buoyancy force will deleteriously affect the flow

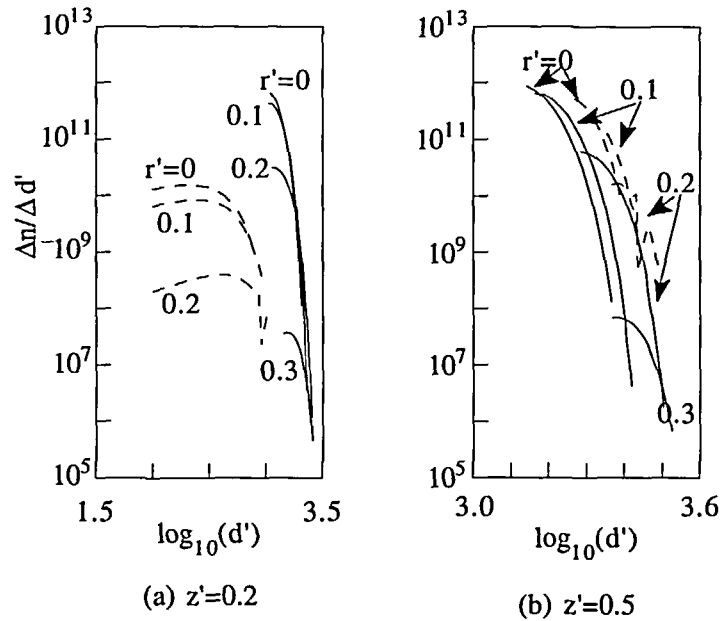


Figure 6 Evolution of particle size distribution with respect to Reynolds number for $D=5$ cm (—, $Re=200$; ---, $Re=10$)

field. Aerosols with a narrow size distribution are formed if the flow conditions in the condenser are laminar and a large mixing in the condenser tube is avoided²¹. The particles generated by nucleation in the circulation region can escape from the circulation region by the thermophoretic force. Figure 6 shows the particle size distribution (PSD) in forced and mixed convection regions. The PSD can not be represented by a specific function even around the exit where vapour condensation has almost ceased. In the Eulerian method, the PSD can be represented by the log-normal function because the numerical diffusion smooths the sharp particle size distribution⁷. However, in the Lagrangian method, the numerical diffusion is absent. Due to the Kelvin effect, the particles, which are generated in the region of $dS/dz < 0$, instantly evaporate in the next downstream position where the critical particle size is larger than the particle size. The maximum particle generation nearly occurs at the point with the minimum critical size, therefore, the particles generated next to the maximum supersaturation do not contribute to the particle number density and the PSD looks like a half-dome. Since the maximum vapour concentration and supersaturation are maintained near the centreline, the maximum particle concentration is obtained in the centre. Larger particles appear near the wall because the region near the wall is rapidly cooled and a particle residence time is large. Nucleation scarcely occurs near the wall. The tube average geometric standard deviation (GSD) of the PSD for $Re=200$ is 1.187 which is larger than 1.157 for $Re=10$. For the uniformity of particle size distribution when seed particles are absent, the mixed convection flow is more favourable than the forced convection flow. With sufficient inlet seed, $n_{in}=10^{10}/\text{m}^3$, where the homogeneous nucleation is fully suppressed, the tube average GSD of the PSD for $Re=200$ is 1.022 which is smaller than 1.107 for $Re=10$. Therefore, with sufficient inlet seed, it is found that the forced convection flow is more favourable than the mixed convection flow for aerosols with a narrow size distribution.

The number concentrations of Na_2SO_4 particles produced by the homogeneous nucleation are shown with respect to the Reynolds number in Figure 7(a). In case that inlet seed is absent, the number density of the tube average around the tube inlet is larger than that of the centreline

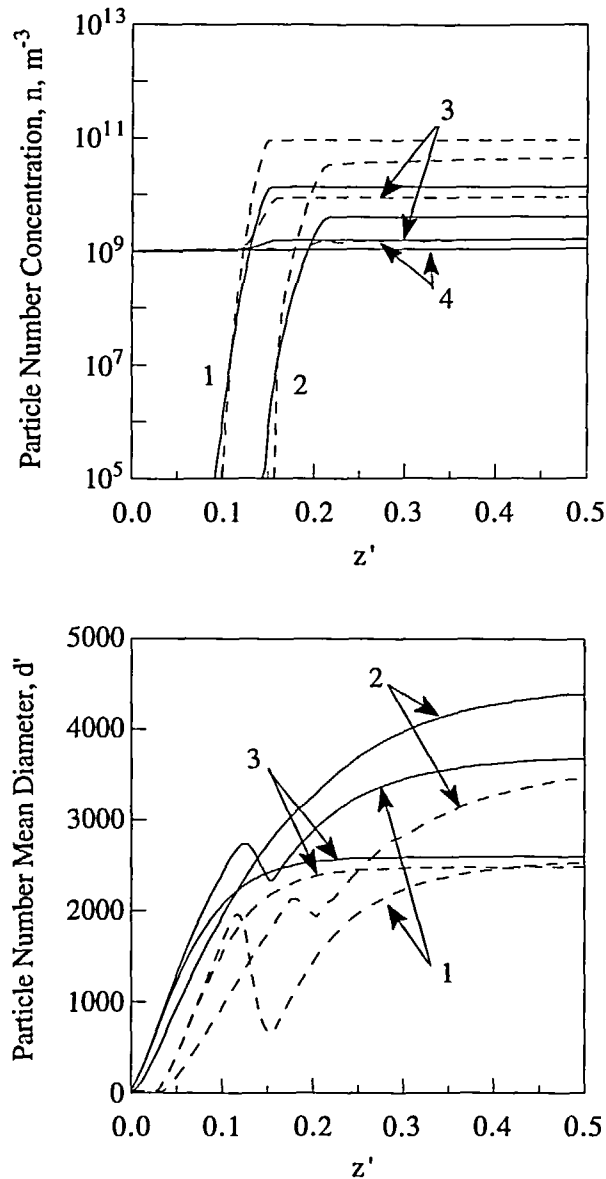


Figure 7 Evolution of mixing-cup average and centreline particle number concentration (a) (1, $Re=200$ without seed particles; 2, $Re=10$ without seed particles; 3, $Re=200$ with seed particles, $n_{i,m} = 10^9/m^3$; 4, $Re=10$ with seed particles, $n_{i,m} = 10^9/m^3$) and number mean diameter (b) (1, $Re=200$ with seed particles, $n_{i,m} = 10^{10}/m^3$) along the condenser length with respect to Reynolds number for $D=5$ cm (—, tube average value; ---, centreline value)

because cooling starts around the wall, and the homogeneous nucleation firstly occurs near the wall. Along the downstream, the total number density is governed by the particles generated around the centreline. The number density becomes constant where the nondimensional axial distance is larger than 0.1 for $Re=200$, 0.15 for $Re=10$. On those points which nearly coincide with the region of the $dS/dz=0$, the particle mass fraction increases considerably. With inlet

seed, $n_{i,n} = 10^9/\text{m}^3$, curves 3 and 4 in *Figure 7(a)*, the particle number density slightly increases from the point where the particle number density line without seed particles crosses the seed number density line. Since homogeneous nucleation is suppressed by the vapour condensation to seed particles, the total number density at the outlet is smaller than that only for homogeneous nucleation. The dimensionless number mean diameters of the particles are shown in *Figure 7(b)* in case with seed particles. For $Re = 200$ and $n_{i,n} = 10^9/\text{m}^3$, curve 1, the particle size increases and decreases sharply and thereafter increases gradually. The reason is that, as shown in *Figure 7(a)*, at the early stage the particle number density is constant as the same value of inlet seed concentration and particles grow continuously when their sizes are larger than the critical nucleation size. From around $z' = 0.12$ the homogeneous nucleation becomes dominant, thereby, mean particle size becomes small. From $z' = 0.15$ the particle number density increment by the homogeneous nucleation is nearly negligible and only particle growth continues to the exit, therefore, the particle size increases gradually. For $Re = 10$ and $n_{i,n} = 10^9/\text{m}^3$, as shown in *Figure 7(b)*, the mode of centreline particle size distribution is same as for $Re = 200$ because the particle number concentration in the centreline slightly increases in *Figure 7(a)*. For $Re = 200$ and $n_{i,n} = 10^{10}/\text{m}^3$, the homogeneous nucleation is fully suppressed and the mean particle size is governed only by seed particle growth, and the particle size increases monotonically. Also the difference between the tube average and the centreline particle number mean size is smaller than that in which homogeneous nucleation is not fully suppressed. When inlet seeds are present and the homogeneous nucleation is not fully suppressed, the total particle number concentration is smaller than that only for homogeneous nucleation.

Influence of tube diameter

Figures 8, 9, 10, 11 show the effects of the tube diameter in the condenser with the Reynolds number set to 200. For the same Reynolds number and nondimensional tube length, as the tube diameter increases, the characteristic flow residence time in the tube increases, and the time for

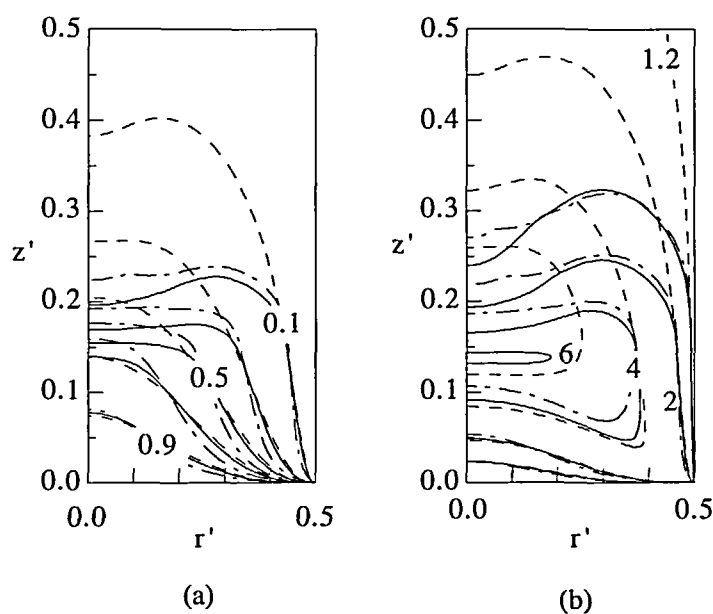


Figure 8 Vapour concentration (ω'_i) (a) and supersaturation ratio (S) (b) isopleths with respect to tube diameter for $Re = 200$ without seed particles (---, $D = 15$ cm; —, $D = 10$ cm; -.-, $D = 2.5$ cm)

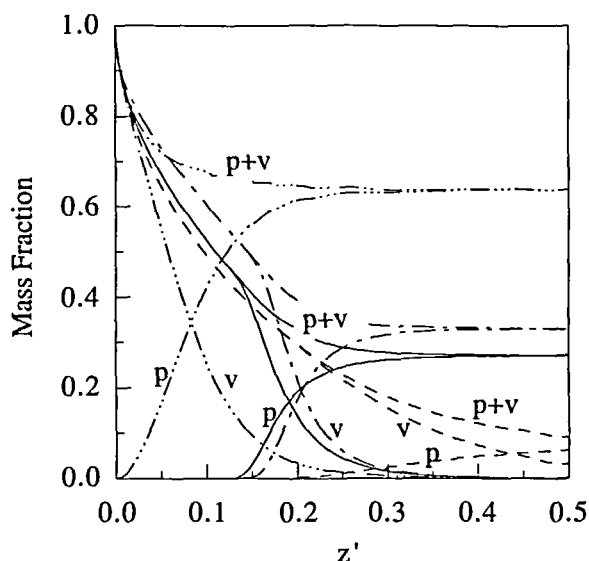


Figure 9 Evolution of particles and vapour mass fraction along the condenser length with respect to tube diameter for $Re=200$ (—, $D=15$ cm without seed particles; —, $D=10$ cm without seed particles; ---, $D=2.5$ cm without seed particles; - - - - , $D=10$ cm with seed particles, $n_{i,m} = 10^9/\text{cm}^3$; 0, particle mass fraction (ω'_p); v, vapour mass fraction (ω'_v); p+v, particle+vapour mass fraction ($\omega'_p + \omega'_v$))

vapour to particle condensation increases, and the number flux of particles increases in (8)–(9). Therefore, the vapour is more rapidly exhausted in the downstream direction, and, thereby, the nucleation is quickly ceased in the further nondimensional downstream region.

In Figure 8, as the tube diameter increases, vapour begins condensing in the core of the tube before significant radial diffusion occurs because vapour to particle condensation increases. Therefore, the vapour concentration fronts are more flattened and the vapour is more rapidly exhausted in the downstream direction. But the vapour concentration for $D=15$ cm is more slowly reduced than that for $D=10$ cm because of the mixed convection effects. As the tube diameter increases, the region of maximum supersaturation decreases because, as above mentioned, the residence time for particles and the particle flux increase, and the vapour to particle condensation becomes large.

In Figure 9, near the inlet, as the tube diameter increases, the vapour wall loss decreases and the vapour concentration is maintained at large value because of the effect of mixed convection. The tube average total and particle mass fractions increase at the exit as the tube diameter increases. The particle mass fraction for large tube diameter firstly increases except for $D=15$ cm where the effect of mixed convection is dominant. In case of $D=2.5$ cm, since the particle flux and particle residence time in the tube are very small, particle mass fraction increases for later. For $D=10$ cm with $n_{i,m} = 10^9/\text{m}^3$, where homogeneous nucleation is fully suppressed, particle mass fraction is very large and vapour wall loss is small since vapour is sufficiently scavenged by particles which have the small mobility.

Without seed particles, the sizes of particles at the exit increases as the tube diameter increases and the PSD mode is the same in Figure 10. Near the wall, because of the vapour diffusion to the wall, the nucleation is suppressed and the particle velocity is very small, thereby, the particle size becomes large. The GSD of the PSD for $D=10$ cm is 1.174 which is larger than 1.167 for $D=15$ cm. In case with seed particles, $n_{i,m} = 10^9/\text{m}^3$, in which homogeneous nucleation is fully suppressed, the GSDs of the PSD are 1.053 for $D=10$ cm and 1.077 for $D=15$ cm. Therefore,

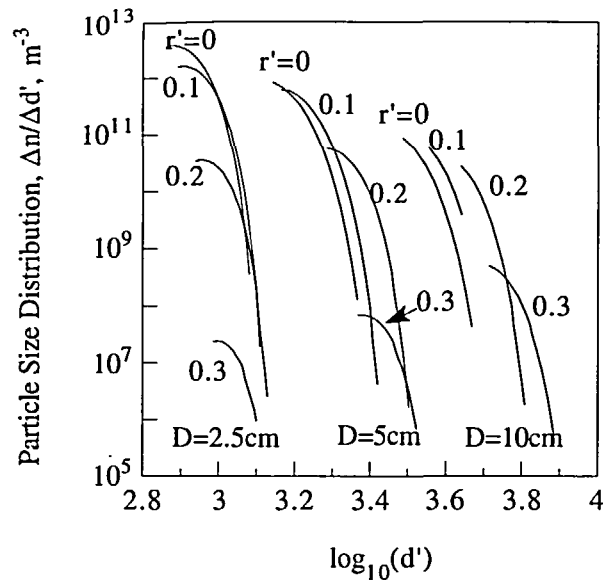


Figure 10 Evolution of particle size distribution with respect to tube diameter without seed particles for $Re = 200$ at $z' = 0.5$

it is clearly indicated that the homogeneity of the PSD becomes better with sufficient seed particles. However, in case of $n_{i,m} = 10^9/m^3$ and $D = 5$ cm in which the homogeneous nucleation is not fully suppressed, the GSD value of PSD is 1.383 which is larger than the value only for the homogeneous nucleation.

In case without seed particles, particle generation starts late for $D = 15$ cm because of the mixed convection. As the tube diameter increases, the particles number density in far downstream decreases in Figure 11(a) and the number mean size of particles increases in Figure 11(b). In Figure 11(b), the tube average particle size is larger than that around the centreline in which homogeneous nucleation occurs actively and the particle number concentration is high. In the upstream region, the particle diameter shows the irregular increment rates. At the early stage when the new particle formation rate is small, the particle growth effect is larger than nucleation effect, but when the nucleation effect becomes large, the particle size is governed by the particle generation. Later, the nucleation is suppressed and the size is controlled by particle growth. When the vapour is nearly exhausted, the particle size becomes constant. This trend can be found in Pratsinis's work²². With seed particles, $n_{i,m} = 10^9/m^3$, for $D = 10$ cm, where homogeneous nucleation is fully suppressed, the tube average and centreline number density is constant in Figure 11(a). In Figure 11(b), the particle size increases monotonically. Also, in this case, the particle size is larger than that only for homogeneous nucleation, the reason is that, as shown in Figure 9, the wall loss is small and, as shown in Figure 11(a), the particle concentration is small. The particles near the centreline starts to grow in the downstream ($z' = 0.03$) where seed particle size is larger than the critical nucleation size. In case with seed particles, the size difference between the tube average and the centreline is smaller than that in the case only for homogeneous nucleation. This is also related to improvement of the GSD of the PSD. The mean particle diameter increases as the tube diameter increases in Figure 11(b). The tube average particle size is larger than that around the centreline because the gas temperature near the wall is lower. With seed particles, the particles grow early and the size of the particle is larger than that for homogeneous nucleation because the particle number density is smaller than that for homogeneous nucleation in Figure 11(a).

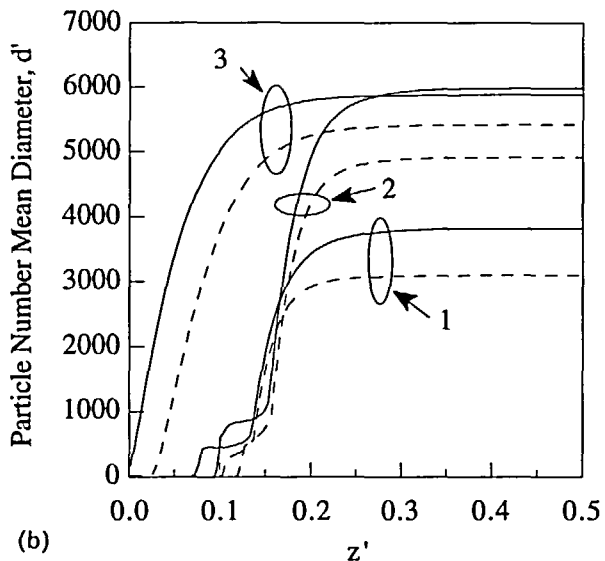
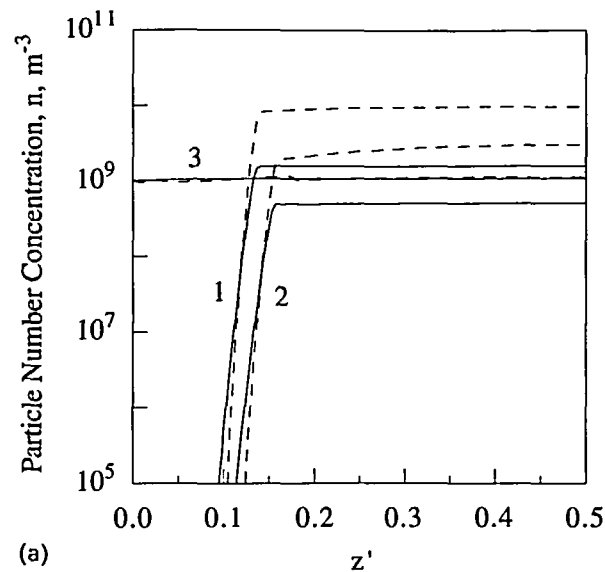


Figure 11 Evolution of mixing-cup average and centreline particle number concentration (a) and number mean diameter (b) along the condenser length with respect to tube diameter for $Re = 200$ (1, $D = 10$ cm without seed particles; 2, $D = 15$ cm without seed particles; 3, $D = 10$ cm with seed particles, $n_{in} = 10^9/cm^3$. —, tube average value; ---, centreline value)

CONCLUSIONS

We have presented the equations for condensation in cooled laminar tube flows and considered their solution for low vapour concentrations and variable vapour-gas thermodynamic properties. The main new results of this paper are those for particles which include the effects of mixed convection. We treated the problem, including coupling with the aerosol size distribution, by PSI-CELL method. When inlet seed concentration is absent, total vapour wall loss increases

and the particle number concentrations decrease as the Reynolds number decreases with the same tube diameter although the effects of the mixed convection decrease the vapour diffusion to the wall near the tube inlet. In this numerical analysis, the PSD mode locally can not be represented by a specific function. As the tube diameter increases in the same Reynolds number, the vapour wall loss decreases and particles number density in far downstream decreases. With seed particles in which homogeneous nucleation is fully suppressed, the vapour wall loss is very small and the homogeneity of the PSD is improved.

REFERENCES

- 1 Friedlander, S. K. *Smoke, Dust and Haze*, Wiley, New York (1977)
- 2 Pesthy, A. J., Flagan, R. C. and Seinfeld, J. H. Theory of aerosol formation and growth in laminar flow, *J. Colloid Interface Sci.*, **91**, 525-545 (1983)
- 3 Seigneur, C., Hudischewskyj, A. B., Seinfeld, J. H., Whitby, K. T., Whitby, E. R., Brock, J. R. and Barnes, H. M. Simulation of aerosol dynamics: a comparative review of mathematical models, *Aerosol Sci. Technol.*, **5**, 205-222 (1986)
- 4 Kim, Y. P. and Seinfeld, J. H. Simulation of multicomponent aerosol condensation by the moving sectional method, *J. Colloid Interface Sci.*, **135**, 185-199 (1990)
- 5 Warren, D. R. and Seinfeld, J. H. Simulation of aerosol size distribution evolution in systems with simultaneous nucleation, condensation, and coagulation, *Aerosol Sci. Technol.*, **4**, 31-43 (1985)
- 6 Phanse, G. M. and Pratsinis, S. E. Theory for aerosol generation in laminar flow condensers, *Aerosol Sci. Technol.*, **11**, 100-109 (1989)
- 7 Im, K. H., Ahluwalia, R. K. and Chung, C. F. RAFT: A computer model for formation and transport of fission product aerosol in LWR primary systems, *Aerosol Sci. Technol.*, **4**, 125-140 (1985)
- 8 Japuntich, D. A., Stenhouse, J. I. T. and Liu, B. Y. H. Conditions for monodispersity of heterogeneous condensation aerosols using dimensionless groups, *J. Colloid Interface Sci.*, **136**, 393-400 (1990)
- 9 Crowe, C. T., Sharma, M. P. and Stock, D. E. The particle-source-in cell (PSI-CELL) model for gas-droplet flows, *ASME Trans., J. Fluids Engineering*, **99**, 325-332 (1977)
- 10 White, F. M. *Viscous Fluid Flow*, McGraw Hill (1974)
- 11 Pratsinis, S. E. and Kim, K. S. Particle coagulation, diffusion and thermophoresis in a laminar tube flows, *J. Aerosol Sci.*, **20**, 101-111 (1989)
- 12 Fuchs, N. A. and Sutugin, A. G. *High-Dispersed Aerosols*, G. M. Hidy and J. R. Brocks (Eds.). *Topics in Current Aerosol Research*, Pergamon, New York, 1-60 (1971)
- 13 Talbot, L., Cheng, R. K., Schefer, R. W. and Willis, D. R. Thermophoresis of particles in a heated boundary layer, *J. Fluid Mech.*, **101**, 737-758 (1980)
- 14 Reid, R. C., Prausnitz, J. M. and Sherwood, T. K. *The Properties of Gases and Liquids*, McGraw-Hill (1977)
- 15 Patanker, S. V. *Numerical Heat Transfer and Fluid Flow*, McGraw-Hill (1980)
- 16 Marner, W. J. and McMillan, H. K. Combined free and forced laminar convection in a vertical tube with constant wall temperature, *ASME Trans. J. Heat Transfer*, **92**, 559-562 (1970)
- 17 Stratmann, F. and Whitby, E. R. Numerical solution of aerosol dynamics for simultaneous convection, diffusion and external forces, *J. Aerosol Sci.*, **20**, 437-440 (1989)
- 18 Walker, K. L., Homsy, G. M. and Geyling, F. T. Thermophoretic deposition of small particles in laminar tube flow, *J. Colloid Interface Sci.*, **69**, 138-147 (1979)
- 19 Gelbard, F. Modeling multicomponent aerosol particle growth by vapor condensation, *Aerosol Sci. Technol.*, **12**, 399-412 (1990)
- 20 Pratsinis, S. E., Kodas, T. T. and Sood, A. Design of laminar flow condensers for production of monodisperse aerosols, *Ind. Eng. Chem. Res.*, **27**, 105-110 (1988)
- 21 Stahlhofen, W., Gebhart, J. and Roth, C. Generation and properties of a condensation aerosol of di-2-ethylhexylsebacate (DES)-III: experimental investigations into the process of aerosol formation, *J. Aerosol. Sci.*, **7**, 223-231 (1976)
- 22 Pratsinis, S. E. Simultaneous nucleation, condensation, and coagulation in aerosol reactors, *J. Colloid Interface Sci.*, **124**, 416-427 (1988)